

## Article

# Orthogonally Polarized Dual-Wavelength Gain-Switched Ho:LuLiF<sub>4</sub> Pulse Laser

Guanqu Hu<sup>1</sup>, Jinhui Cui<sup>1</sup>, Fengjun Tian<sup>1</sup> , Zhengxin Gao<sup>1</sup>, Shixiong Yan<sup>1</sup>, Sichen Liu<sup>1</sup>, Xinlu Zhang<sup>2,\*</sup> and Li Li<sup>1,3,\*</sup> 

<sup>1</sup> Key Laboratory of In-Fiber Integrated Optics of Ministry of Education, Harbin Engineering University, Harbin 150001, China

<sup>2</sup> School of Physical Science and Technology, Tiangong University, Tianjin 300387, China

<sup>3</sup> School of Physics, Harbin Institute of Technology, Harbin 150001, China

\* Correspondence: zhangxinlu@tiangong.edu.cn (X.Z.); lylee\_heu@hrbeu.edu.cn (L.L.)

**Abstract:** A compact, orthogonally polarized, gain-switched a-cut Ho:LuLiF<sub>4</sub> laser with intra-cavity pumping by a self-Q-switched Tm:YAP laser is demonstrated here for the first time. The  $\pi$ -polarization laser at 2052 nm and  $\sigma$ -polarization laser at 2066 nm were experimentally observed with the maximum output power values of 299 mW and 126 mW, respectively, and the two polarization directions were always kept mutually orthogonal as the pump power increased. The ratio of the output power between the two orthogonal polarization lasers was nearly 1:1 at a pump power of 18.4 W. The minimum pulse width of the Ho:LLF laser was 326 ns, the maximum repetition rate was 24 kHz, and the maximum average energy was 28  $\mu$ J.

**Keywords:** orthogonally polarized laser; Ho:LuLiF<sub>4</sub>; dual-wavelength



**Citation:** Hu, G.; Cui, J.; Tian, F.; Gao, Z.; Yan, S.; Liu, S.; Zhang, X.; Li, L.

Orthogonally Polarized Dual-Wavelength Gain-Switched Ho:LuLiF<sub>4</sub> Pulse Laser. *Photonics* **2023**, *10*, 62. <https://doi.org/10.3390/photonics10010062>

Received: 5 December 2022

Revised: 31 December 2022

Accepted: 4 January 2023

Published: 6 January 2023



**Copyright:** © 2023 by the authors. Licensee MDPI, Basel, Switzerland. This article is an open access article distributed under the terms and conditions of the Creative Commons Attribution (CC BY) license (<https://creativecommons.org/licenses/by/4.0/>).

## 1. Introduction

Ultrafast lasers operating in the 2  $\mu$ m eye-safe spectrum waveband have attracted much attention for a variety of applications in differential absorption lidars, coherent Doppler wind lidars, remote sensing, laser medicine, and nonlinear frequency conversion in the mid-infrared band [1–6]. Both Tm<sup>3+</sup> and Ho<sup>3+</sup> ion-doped lasers are able to generate lasers in the 2  $\mu$ m band. Compared with Tm-doped lasers, Ho-doped lasers can achieve higher optical-to-optical conversion efficiencies, theoretically close to 95%. The optical-to-optical conversion efficiency of single-doped Ho lasers is also significantly higher than that of the widely used Tm and Ho co-doped lasers (the theoretical limit is below 45%) [7]. Single Ho-doped laser crystals have the advantage of high-energy storage, which provides a reliable guarantee of high-energy laser output. Compared with single Tm-doped and Tm–Ho co-doped laser crystals, single Ho-doped laser crystals possess a larger excited emission cross-section (the emission cross-section of Ho ions is about five times larger than that of Tm ions), a long fluorescence lifetime, and a long upper energy level lifetime (~10–16 ms), which facilitates energy storage for Q-switched laser output and is less likely to cause damage to materials [8–11]. Among the Ho-doped crystals that have received widespread attention such as aluminate crystals (YAG/YAP), silicate crystals (Re<sub>2</sub>SiO<sub>5</sub>), tungstate crystals (KY(WO<sub>4</sub>)<sub>2</sub>), and fluoride crystals (LiYF<sub>4</sub>), fluoride crystals usually have smaller phonon energies and larger energy level lifetimes. Ho:LuLiF<sub>4</sub> (Ho:LLF) crystals, as members of the fluoride crystal family, can be used in excellent single Ho-doped lasers. In Ho:LLF, the larger ionic radius of the matrix Lu<sup>3+</sup> ions can generate a stronger crystal field and induce the doped Ho ions to form a larger amount of energy level splitting, which results in Ho:LLF having a wider spectral range and a lower laser threshold [7,12]. Ho:LLF crystals belong to the tetragonal crystal system and possess two polarization directions, namely the electric field E//a axis of the  $\sigma$ -polarization direction and the  $\pi$ -polarization direction of the E $\perp$ a axis. Both directions can produce linearly polarized laser output.

LLF crystals have higher natural birefringence characteristics and lower upconversion efficiency in lasers compared with YAP and YAG crystals [13]. Additionally, Ho:LLF crystals have good thermo-optical and thermomechanical properties. For Ho:LLF crystals, the thermal conductivity (a-axis) is  $4.3 \text{ Wm}^{-1}\text{K}^{-1}$ , the linear expansion coefficient (c-axis) is  $11 \times 10^{-6} \text{ K}^{-1}$ , and the thermal coefficient of refractive index  $dn/dT$  (c-axis) is  $-3.6 \times 10^{-6} \text{ K}^{-1}$  [7]. Ho:LLF crystals have many features such as a low upconversion loss, negative thermo-optical coefficient, high resistance to optical damage, and no thermally induced birefringence. These excellent features make Ho:LLF crystals attractive for applications in  $2 \mu\text{m}$  lasers and optical amplifiers [14]. Recently, Ho:LLF lasers operating in the continuous wave and Q-switched modes were studied [15,16]. However, the co-existence of dual wavelengths for orthogonal polarizations in a gain-switched Ho:LLF pulse laser has not been investigated.

An orthogonally polarized laser oscillates two adjacent longitudinal modes with a mutually perpendicular polarization state, with the wavelength (or frequency) difference between the two orthogonally polarized longitudinal modes resulting in a dual-wavelength laser. An orthogonally polarized dual-wavelength laser has a remarkable physical characteristic: the laser wavelength (or frequency) interval can be continuously tuned from tens of MHz to one longitudinal mode interval (several GHz) or even more. Dual-wavelength lasers have been extensively and intensively used in lidars, terahertz research, nonlinear frequency conversion and the generation of multiple types of solitons in fiber lasers, precision laser spectroscopy, and medical applications [6,17,18]. Orthogonal polarization lasers have been a hot item of international interest. In 2010, X. P. Yan et al. developed a 26.2 W orthogonally linearly polarized Nd:YVO<sub>4</sub> laser by adopting two c-axis orthogonally a-cut bonded YVO<sub>4</sub>/Nd:YVO<sub>4</sub> crystals. Each end face of the laser crystals was pumped by a diode laser, which allowed for the more efficient generation of orthogonally polarized linearly polarized lasers and equalized the energy of the dual-wavelength output laser [19]. In 2015, Z. Jing et al. selected the Nd:LiYF crystal as the gain medium and theoretically analyzed the conditions for simultaneous  $\pi$ - and  $\sigma$ -polarized emissions from the four-level transition in Nd<sup>3+</sup>. An orthogonally polarized dual-wavelength laser at 1047, and 1053, 1321, and 1313 nm was operated in the stable CW mode by using a simple linear resonator [20]. For the  $2 \mu\text{m}$  waveband, Segura et al. reported emissions operating simultaneously in the CW mode at 1922 and 1946 nm by using a Tm:KLu(WO<sub>4</sub>) crystal. The polarization switching of a Tm:KLu(WO<sub>4</sub>) laser was shown with an increased pump power [21]. X. L. Zhang et al. studied the switching of orthogonal polarizations and optical bistability in a Tm–Ho:LLF laser. The switching of the  $\pi$ -polarization at 2069 nm and  $\sigma$ -polarization at 2066 nm were experimentally observed [22]. Previous studies on dual-wavelength, orthogonally polarized lasers have mostly focused on lasers operating in the  $1 \mu\text{m}$  waveband or Tm and Ho co-doped lasers in the  $2 \mu\text{m}$  waveband [22–25]. However, there have been no experimental studies of the polarization characteristics of single Ho-doped LLF lasers at  $2 \mu\text{m}$ .

In this paper, we demonstrate the polarization coexistence between two orthogonal polarizations of a gain-switched Ho:LLF laser. A compact intra-cavity pumped construction was adopted, and the gain-switched Ho:LLF pulse laser was obtained from a self-Q-switched Tm:YAP laser without extra Q-switched components. In this experiment, the output power of two orthogonal polarization lasers was simultaneously and individually measured. The polarization characteristics of the gain-switched Ho:LLF laser and the energy ratio between two orthogonal polarization lasers are presented.

## 2. Experimental Setup

For more resonant pump energy, a more compact and simple laser system with two gain mediums was used in this experiment. Figure 1 shows a simple plane-concave cavity configuration. A fiber-coupled diode laser at 795 nm was used as the pump laser. The diameter of the fiber core was  $400 \mu\text{m}$ , and the numerical aperture (NA) was 0.22. The maximum pump power of the fiber-coupled diode laser was 30 W. The pump light emitted by the diode laser was linearly polarized, and the polarization direction was perpendic-

ular to the cavity axis. To obtain a self-Q-switched laser, the diode laser pump spot was collimated and focused in the Tm:YAP crystal by a 1:2 coupling lens group with a focal length of 75 mm, and the distance between the crystal and the coupling lens group was 74 mm. Optimizing the pump spot on the gain media by slightly adjusting the position of the coupling lens set was the best way to maximize the output power. The Tm:YAP crystal and the Ho:LLF crystal were placed inside the cavity in sequence. The dimensions of the b-cut Tm:YAP crystal with a 5% dopant concentration was  $3 \times 3 \times 10 \text{ mm}^3$ , and the a-cut Ho:LLF crystal had a dopant concentration of 0.5% with dimensions of  $3 \times 3 \times 5 \text{ mm}^3$ . Two laser crystals were covered with indium foil and fitted on a water-cooled copper holder. The temperature of the cooling water was maintained at 291 K. The distance between the Tm:YAP crystal and the Ho:LLF crystal was 10 mm. Both end faces of the Tm:YAP crystal were high-transmission ( $T > 99.5\%$ ) coated at 1.9–2.1  $\mu\text{m}$  and 795 nm. Regarding the Ho:LLF crystal, the dichromatic coatings on the both of its end faces were high-transmitting in the 1900–2100 nm wavelength range. A compact linear resonator was adopted between the input plane mirror and output concave mirror. The total length of the cavity was about 155 mm. The dichroic input plane mirror (M1) coating on both end faces was high-transmitting at 780–800 nm, but it was totally reflecting at 1.9–2.1  $\mu\text{m}$ . A plane-concave mirror, which was partially reflective ( $T = 5\%$ ) at 1.9–2.1  $\mu\text{m}$ , was used as the output mirror (M2). The curvature radius of the output mirror (M2) was 200 mm. A broadband polarizing beam splitter (PBS) at 1.9–2.1  $\mu\text{m}$  (extinction ratio  $T_p:T_s > 1000:1$ ) was placed behind the output mirror (M2) to split the output laser into two orthogonal polarizations.

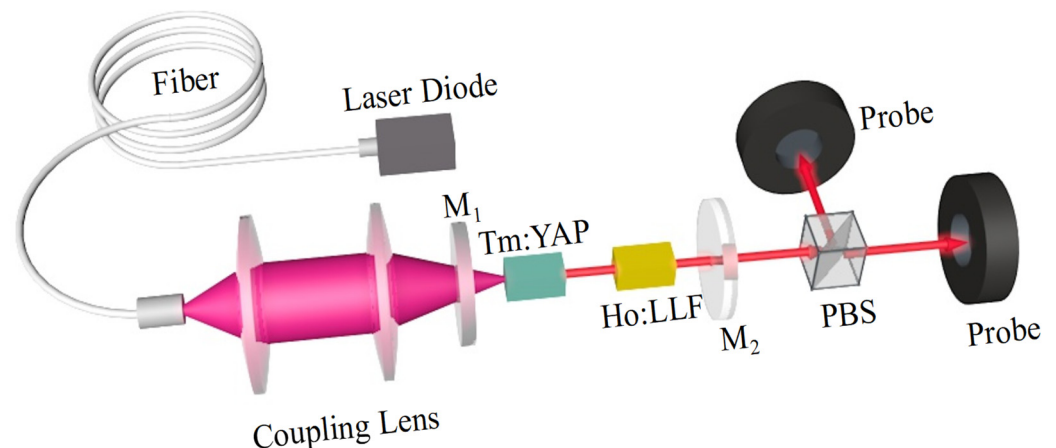


**Figure 1.** Experimental setup of the orthogonally polarized Ho:LLF laser.

The output power was measured with a Coherent FieldMaxII laser power meter and an InGaAs photodiode. The laser spectrum was monitored with a Zolix monochromator (Omni- $\lambda$  3015; the resolution of the spectrum was 0.1 nm). A 300 MHz bandwidth digital oscilloscope (Tektronix TDS3032B) was applied to record the output pulse trains with a  $>100$  MHz bandwidth IR detector (Vigo PVM-10.6).

### 3. Experimental Results and Discussion

First, we only inserted the Tm:YAP crystal into the cavity to establish a self-Q-switched Tm:YAP pulsed laser at 1.94  $\mu\text{m}$ . The self-Q-switched Tm:YAP laser operated as the second pump source to activate the Ho:LLF crystal to generate a 2  $\mu\text{m}$  laser. Therefore, the Ho:LLF laser operated in the gain-switched mode. Figure 2a depicts the output power of the Tm:YAP pulse laser without the Ho:LLF crystal in the cavity as the pump power increased. Figure 2b shows pulse trains of the Tm:YAP pulse laser at a pump power of 13.5 W.

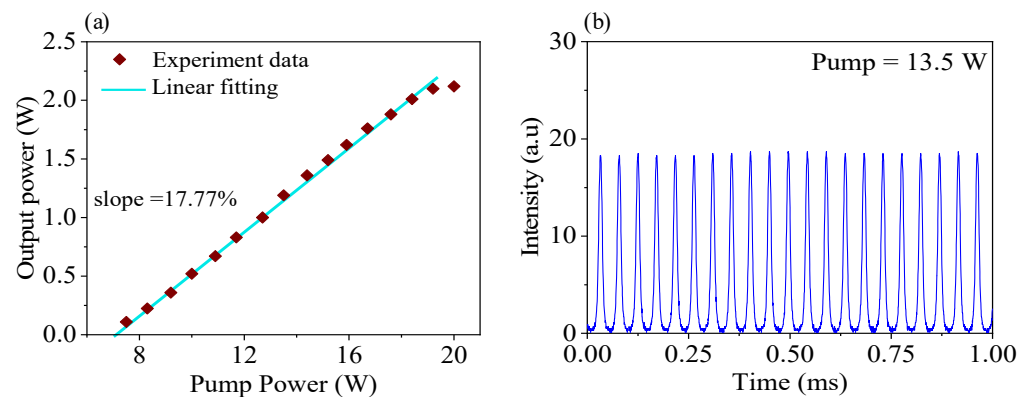


**Figure 2.** (a) Output power of the self-Q-switched Tm:YAP pulsed laser with respect to the incident pump power and (b) pulse trains of the Tm:YAP laser at a pump power of 13.5 W.

The maximum output power of the Tm:YAP laser at 1944 nm was 2.10 W. The slope efficiency was 17.77%. Note that the output power of the self-Q-switched Tm:YAP laser led to a saturable effect after the pump power increased to 20 W, as shown in Figure 2a. As the pump further increased above 20 W, the laser power suddenly dropped and then the laser output terminated due to the possible laser damage of the Tm:YAP crystal. This suggested that significant thermal effects occurred in the Tm:YAP crystal. The pulse laser could steadily operate for several hours. After using a narrow-band filter at 1850–1950 nm to separate the Tm:YAP laser, we measured the repetition rate and pulse width by directly collecting output signals with a digital oscilloscope. The maximum Tm:YAP pulse energy and repetition rate were 28  $\mu\text{J}$  and 47 kHz, respectively, and the minimum Tm:YAP pulse width was 2.5  $\mu\text{s}$ . Because the cavity mode at 1.94  $\mu\text{m}$  was larger than the 795 nm pump region, the ground state reabsorption (GSRA) effect resulted in part of the cavity mode exceeding the pump mode focused on the Tm:YAP crystal, which can accordingly be considered a saturable absorber. This provided an additional loss for the Tm:YAP laser's oscillation. The GSRA effect occurring in the Tm:YAP crystal could modulate the laser's oscillation dynamics, leading to a self-Q-switched pulse laser output [26]. The GSRA effect via  $\text{Tm } ^3\text{H}_6 \rightarrow ^3\text{F}_4$  should be considered in the pumping process of lasers at 795 nm [26]. By using such a self-Q-switched laser, the Ho:LLF crystal can obtain enough intra-cavity energy to emit the laser. Figure 3 shows the energy level diagram of the  $\text{Ho}^{3+} ^5\text{I}_7$  excited manifold and the  $\text{Ho}^{3+} ^5\text{I}_8$  ground manifold of Ho:LLF. The main absorption wavelength of the Ho:LLF crystal was centered around 1940 nm, which corresponded to the emission wavelength of the Tm:YAP crystal. The large size of the  $\text{Lu}^{3+}$  host ion in Ho:LLF resulted in a larger crystal field and the crystal field splitting of the lanthanide ion [13,14]. The emission wavelengths on the  $\pi$ -polarization and  $\sigma$ -polarization in Ho:LLF were 2052 nm and 2066 nm, respectively.

After inserting the Ho:LLF crystal into the cavity, the output performance of the intra-cavity pumped Ho:LLF laser was investigated. To obtain 2  $\mu\text{m}$  orthogonal polarization lasers, we set a small angle between the optical axis of the Ho:LLF laser crystal and the axis of the cavity, which could induce the high natural birefringence of the a-cut Ho:LLF crystal. To accurately measure the output profiles of the Ho:LLF laser, we used a narrow-band filter at 2000–2100 nm wavelengths to eliminate the influence of the pump laser and the Tm:YAP laser on the measurements. By using a polarizing beam splitter (PBS), the two separated orthogonally polarized laser beams were obtained. We measured the output power for individual polarization at the same time. We defined the  $\pi$ -polarization and the  $\sigma$ -polarization as the directions along the c-axis and a-axis of the Ho:LLF crystal, respectively. In order to optimize laser output quality and reduce cavity leakage loss, we compressed the length of the resonator as much as possible. Considering the actual size of the crystal and heat sink in the experiment, as well as the necessity to leave some space to rotate the Ho:LLF crystal at a small angle, the length of the resonator could be

compressed to a minimum of about 155 mm. We conducted optimal output experiments by using Ho:LLF crystals of different lengths (3 mm, 5 mm and 8 mm). Figure 4a shows the variation of output power with pump power for the three different crystal lengths. As shown in Figure 4a, the best result was obtained with the Ho:LLF crystal dimensions of  $3 \times 3 \times 5 \text{ mm}^3$ . The total output power and the output power for the individual polarization directions were measured by increasing the pump power. While increasing the pump power from zero to threshold power at  $P_{\pi\text{-thr}} = 13.5 \text{ W}$ , the output power varied from zero to 26.7 mW. Figure 4b,c, respectively, shows the total output power and the output power for the individual polarization directions of the Ho:LLF (crystal length of 5 mm) laser with respect to the incident pump power. When pump power increased above the threshold, the output laser was only  $\pi$ -polarized at 2052 nm, and the maximum output power was 299 mW when the pump power was 15.9 W. After increasing pump power from  $P_{\pi\text{-thr}}$  to  $P_{\pi\text{-max}} = 15.9 \text{ W}$ , the output power for  $\pi$ -polarization in the Ho:LLF laser decreased. When the pump power increased from  $P_{\sigma\text{-thr}} = 16.3 \text{ W}$  to 18.8 W, the  $\sigma$ -polarization laser at 2066 nm began oscillating and the output power for  $\sigma$ -polarization increased from zero to maximum power  $P_{\sigma\text{-max}} = 126 \text{ mW}$ . By inserting two laser crystals into the cavity, the laser of the Tm:YAP crystal could not only be used as a pump source to provide gain to the Ho:LLF crystal but also control the losses of the orthogonal polarizations in the Ho:LLF laser based on the excellent anisotropy of the Tm:YAP crystal. Therefore, the variation of the output power of the two orthogonally polarized laser could be controlled by changing the energy of the Tm:YAP laser. Because of the tiny angle between the optical axis of Ho:LLF and the axis of the cavity, the Ho:LLF laser could emit two orthogonally polarized lasers based on the high natural birefringence of the Ho:LLF crystal [7,25]. In addition, the  $^5I_7 \rightarrow ^5I_8$  energy level transition resulted in 2052 and 2066 nm laser lines. These two laser lines shared a common upper level. The gain competition between 2052 and 2066 nm is not negligible, especially when the pumping power is further increased [23]. Figure 4c shows that when increasing the pump power from  $P_{\sigma\text{-thr}}$ , the output laser energy for the  $\pi$ - and  $\sigma$ -polarizations tended to enter the equilibrium zone. The output power of the  $\pi$ -polarization (2052 nm) was almost the same as the output power of the  $\sigma$ -polarization (2066 nm) when the pump power was 18.4 W.

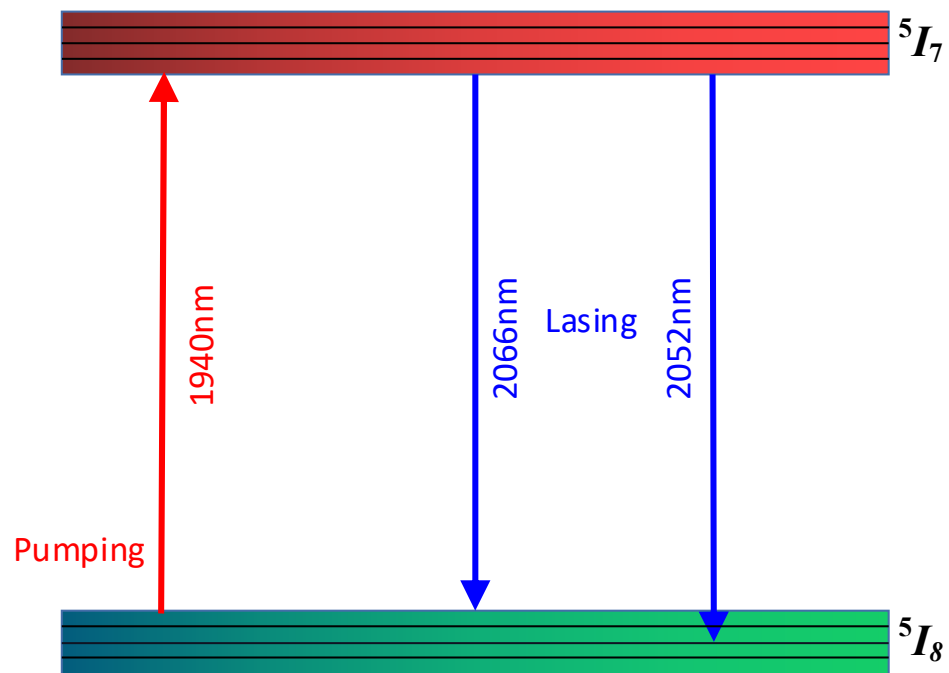
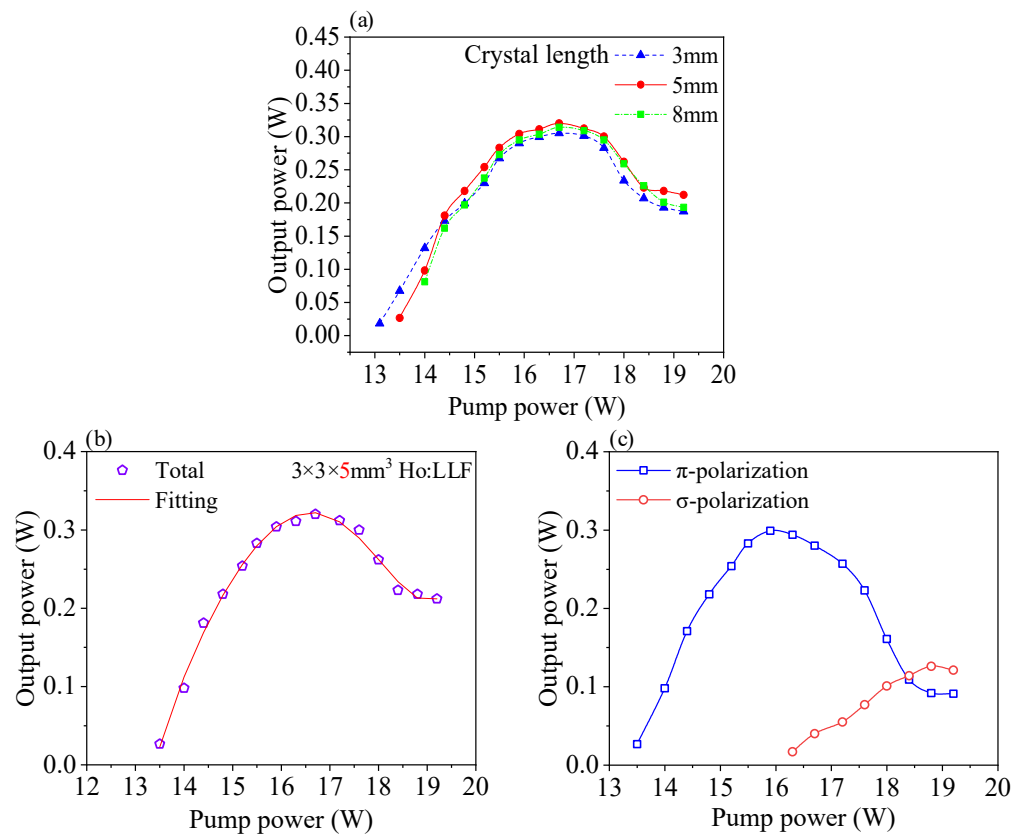
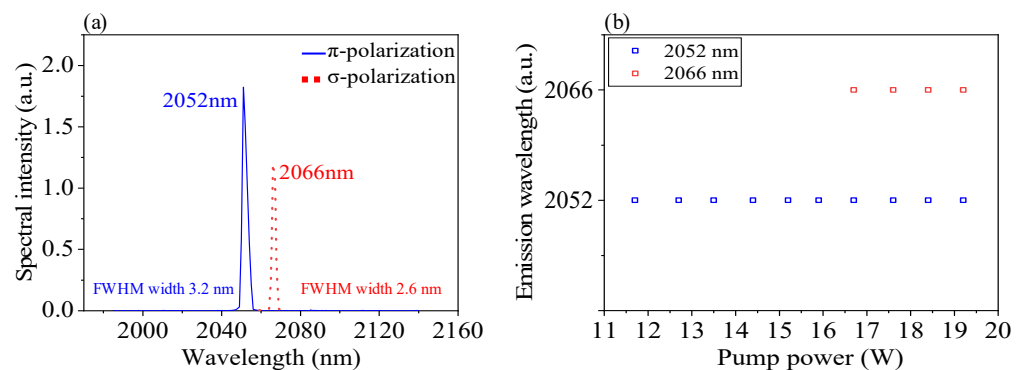


Figure 3. Energy levels in the Ho:LLF crystal [13,14].



**Figure 4.** (a) The output power and pump power for different crystal lengths (3 mm, 5 mm, and 8 mm); (b) the total and (c) individual polarization direction output power in the Ho:LLF (crystal length was 5 mm) laser as a function of the incident pump power.

The measured spectra for the  $\pi$ -polarization and the  $\sigma$ -polarization of the Ho:LLF laser are shown in Figure 5a. The central wavelengths were 2052 nm and 2066 nm for the orthogonal  $\pi$ - and  $\sigma$ -polarizations, respectively. The variation of the emission wavelength for the gain-switched Ho:LLF laser can be explained in the process of intra-cavity gain variation by increasing the pump power, as shown in Figure 5b. With increases in the pump power, the 2052 nm and 2066 nm spectral widths for the  $\pi$ - and  $\sigma$ -polarization emission laser lines, respectively, began to increase due to decreases in the pulse width [27]. The full width at half maximum (FWHM) of the 2052 nm and 2066 nm wavelengths for the orthogonal polarizations were 3.2 nm and 2.6 nm, respectively, as shown in Figure 5a.



**Figure 5.** (a) Optical spectra of the orthogonally polarized dual-wavelength Ho:LLF laser and (b) emission wavelengths of the Ho:LLF laser with respect to pump power.

In addition, the linearly polarized pump induced the parallel polarization of the self-Q-switched Tm:YAP laser. Then, the polarized Tm:YAP laser’s intra-cavity pumped the

Ho:LLF crystal to produce a parallel  $\pi$ -polarization and a vertical  $\sigma$ -polarization at dual wavelengths of 2052 nm and 2066 nm. The larger stimulated emission cross-section of the  $\pi$ -polarization (along the  $c$ -axis) compared with that of the  $\sigma$ -polarization (along the  $a$ -axis) [18] resulted in different oscillation thresholds at the two orthogonal polarizations and different output energy levels at the dual wavelengths, as shown in Figure 4.

When the pump power was maintained 18.4 W, we rotated a linear polarizer to observe the relation between the angle of polarization and the output power after splitting with the PBS, as shown in Figure 6a. The output energy of the  $\pi$ -polarization and  $\sigma$ -polarization lasers was almost the same as when the pump power was 18.4 W. The angle difference of the output power for the  $\pi$ -polarization and  $\sigma$ -polarization directions was 90 degrees, which means that the polarization direction was mutually orthogonal. The process of energy changes within the laser system allowed the entire laser system to achieve the co-existence of two orthogonally polarized lasers due to gain variation by controlling the pump power.

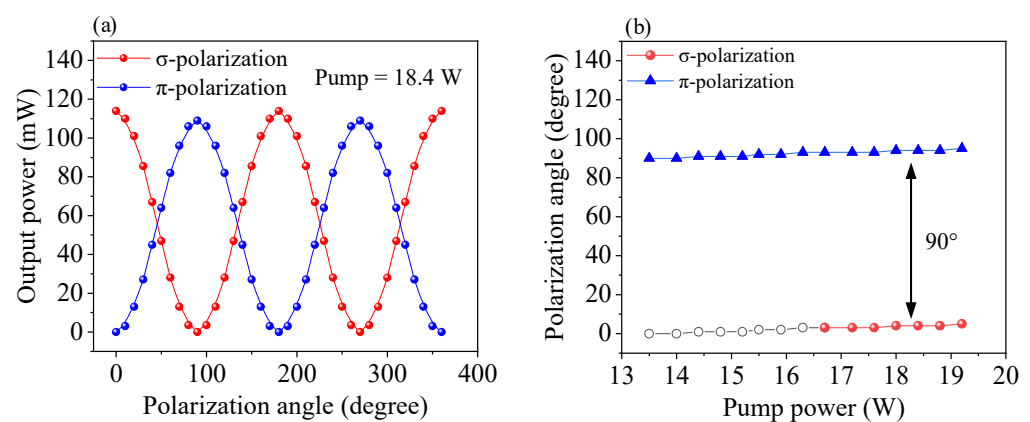


**Figure 6.** (a) The relationship between the angle of polarization and the output power; (b) polarization angles of the orthogonally polarized laser as a function of the pump power.

The variation of the polarization directions in the Ho:LLF laser caused by increases in the pump power is shown in Figure 6b. Because of the high natural birefringence of the  $a$ -cut Ho:LLF crystal, the rotation of the polarization directions of the output power did not occur when the pump power increased [22,23]. Figure 6b shows that the two polarization directions remained mutually orthogonal at all times.

Furthermore, due to the gain-switch between the dual crystals placed into the cavity, the output laser of the Ho:LLF crystal was a pulse laser. Figure 7a,b shows the pulse trains and single pulse shape of the gain-switched Ho:LLF laser when the pump power was 19.2 W. The gain-switched Ho:LLF pulse laser at the 2  $\mu$ m waveband was only obtained with the self-Q-switched Tm:YAP laser. The intensity and period of the gain-switched Ho:LLF laser were stable. The repetition rate and the pulse width of the gain-switched Ho:LLF pulsed laser with respect to the pump power are shown in Figure 8a,b. When increasing the pump power from 13.5 W to 19.2 W, the output pulse energy was insensitive and remained nearly constant at 28  $\mu$ J. The repetition rate gradually increased to the maximum of 24 kHz when the pump power increased to 19.2 W. The minimum pulse width was measured as 326 ns. This increasing tendency occurred because as the pump power increased, the rate of the population inversion density on the upper-level Ho rapidly accumulated and the time required for the population inversion density to reach the threshold was shortened. This led to an increase in the pulse repetition rate and a parallel reduction in the pulse width [28,29]. Due to mechanical and thermal perturbation, the output pulse profile somewhat fluctuated. In this experiment, we employed an air-bearing vibration isolation platform to suppress the fluctuation of the output pulse profiles caused by mechanical vibration. This effectively reduced the uncertainty in the measurements.

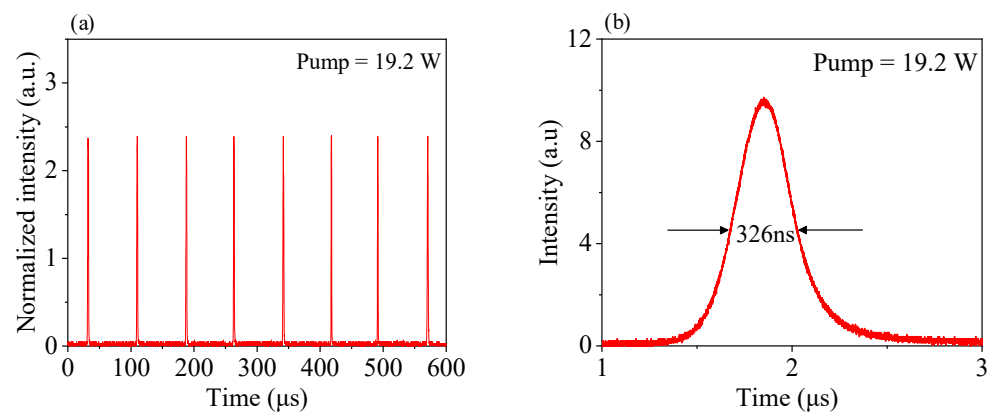


**Figure 7.** (a) Pulse trains and (b) single pulse shape of the gain-switched Ho:LLF laser at a pump power of 19.2 W.

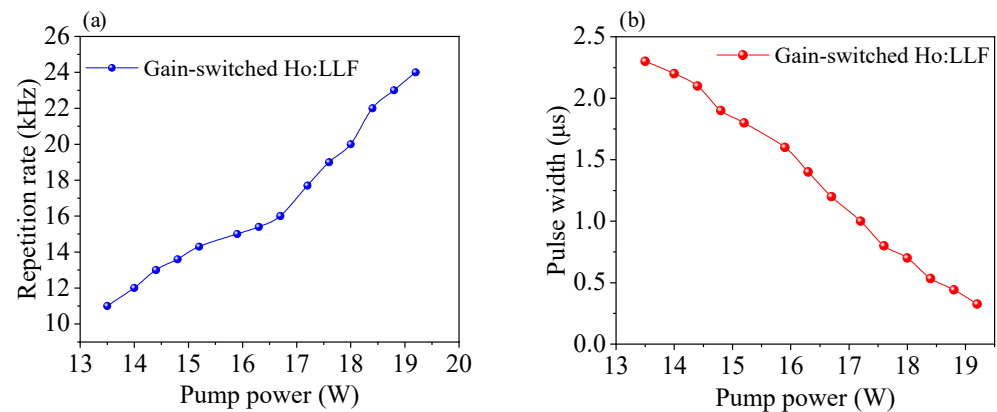


**Figure 8.** (a) Repetition rate and (b) temporal profile of the gain-switched Ho:LLF laser as a function of pump power.

#### 4. Conclusions

In conclusion, we experimentally demonstrated output parameters for  $\pi$ - and  $\sigma$ -polarizations at two different wavelengths in a gain-switched Ho:LLF laser by using an intra-cavity self-Q-switched Tm:YAP laser. The co-existence of the  $\sigma$ -polarized laser at 2066 nm and the  $\pi$ -polarized laser at 2052 nm was achieved by increasing the pump power. The maximum output power for  $\pi$ -polarization (2052 nm) and  $\sigma$ -polarization (2066 nm) was 299 mW and 126 mW at pump power values of 15.9 W and 18.8 W, respectively. The output energy of the two orthogonally polarized states could reach a balanced region in which the output power of the  $\pi$ - and  $\sigma$ -polarization lasers was almost the same when the pump power increased from 18.0 W to 19.2 W. The balanced output energy of the orthogonally polarized dual-wavelength laser could be widely used in differential absorption radars, and the precise measurement of CO<sub>2</sub> and H<sub>2</sub>O in the atmosphere can be achieved via loss-free switching between the dual-wavelength lasers. Regarding the scaling of the output energies of the dual-wavelength laser pulses generated by the Ho:LLF laser, one can make efforts to improve the thermal effects of the Tm:YAP crystal to enhance the intra-cavity pumping power. After measuring the variation of the polarization angle and the increase in pump power, it was found that the two polarization directions were stable and remained orthogonal to each other at all times because of the high natural birefringence of the a-cut Ho:LLF crystal. By using a PBS and other polarized components, we could achieve the switching of the  $\sigma$ -polarization at 2066 nm and the  $\pi$ -polarization at 2052 nm. Furthermore, the minimum pulse width of the gain-switched Ho:LLF laser was about 326 ns, and the maximum pulse energy was 28  $\mu$ J. The pulse repetition rate could be tuned from 11 kHz to 24 kHz by adjusting the pump power. The orthogonally polarized dual-wavelength

gain-switched Ho:LuLiF<sub>4</sub> laser has potential applications in the generation of terahertz waves, as a light source of fiber lasers, and in differential absorption lidars.

**Author Contributions:** Conceptualization, G.H., X.Z. and L.L.; data curation, G.H., Z.G., X.Z. and L.L.; investigation, J.C., X.Z., F.T., L.L. and G.H.; writing—review and editing, G.H., Z.G., J.C., S.Y., S.L., F.T., X.Z. and L.L.; funding acquisition, J.C., F.T., X.Z. and L.L.; formal analysis, L.L.; writing—original draft preparation, G.H.; project administration, J.C. and X.Z.; supervision, L.L. All authors have read and agreed to the published version of the manuscript.

**Funding:** This research was funded by the National Natural Science Foundation of China, grant numbers 61875043 and 72275194, and the 111 Project to the Harbin Engineering University, grant number B13015.

**Institutional Review Board Statement:** Not applicable.

**Informed Consent Statement:** Not applicable.

**Data Availability Statement:** Data underlying the results presented in this paper are not publicly available at this time but may be obtained from the authors upon request.

**Conflicts of Interest:** The authors declare no conflict of interest.

## References

1. Yu, J.; Trieu, B.C.; Modlin, E.A.; Singh, U.N.; Kavaya, M.J.; Chen, S.; Bai, Y.; Petzar, P.J.; Petros, M. 1 J/pulse Q-switched 2 microm solid-state laser. *Opt. Lett.* **2006**, *31*, 462–464. [[CrossRef](#)]
2. Taczak, T.M.; Killinger, D.K. Development of a tunable, narrow-linewidth, cw 2.066- $\mu\text{m}$  Ho:YLF laser for remote sensing of atmospheric CO<sub>2</sub> and H<sub>2</sub>O. *Appl. Opt.* **1998**, *37*, 8460–8476. [[CrossRef](#)]
3. Budni, P.A.; Pomeranz, L.A.; Lemons, M.L.; Miller, C.A.; Mosto, J.R.; Chicklis, E.P. Efficient mid-infrared laser using 1.9- $\mu\text{m}$ -pumped Ho:YAG and ZnGeP<sub>2</sub> optical parametric oscillators. *J. Opt. Soc. Am. B* **2000**, *17*, 723–728. [[CrossRef](#)]
4. Scholle, K.; Lamrini, S.; Koopmann, P.; Fuhrberg, P. 2  $\mu\text{m}$  laser sources and their possible applications. In *Frontiers in Guided Wave Optics and Optoelectronics*; Bishnu, P., Ed.; Intech: London, UK, 2010.
5. He, C.; Killinger, D.K. Dual-polarization modes and self-heterodyne noise in a single-frequency 2.1-microm microchip Ho,Tm:YAG laser. *Opt. Lett.* **1994**, *19*, 396–398. [[CrossRef](#)] [[PubMed](#)]
6. Qi, Y.; Yang, S.; Wang, J.; Li, L.; Bai, Z.; Wang, Y.; Lv, Z. Recent advance of emerging low-dimensional materials for vector soliton generation in fiber lasers. *Mater. Today Phys.* **2022**, *23*, 100622. [[CrossRef](#)]
7. Schellhorn, M. A comparison of resonantly pumped Ho:YLF and Ho:LLF lasers in CW and Q-switched operation under identical pump conditions. *Appl. Phys. B* **2011**, *103*, 777–788. [[CrossRef](#)]
8. Na, Q.X.; Gao, C.Q.; Wang, Q.; Zhang, Y.X.; Gao, M.W.; Ye, Q.; Li, Y. 15 mJ single-frequency Ho:YAG laser resonantly pumped by a 1.9  $\mu\text{m}$  laser diod. *Laser Phys. Lett.* **2016**, *13*, 095003. [[CrossRef](#)]
9. Tang, Y.L.; Xu, L.; Wang, M.J.; Yang, Y.; Xu, X.D.; Xu, J.Q. High-Power gain-switched Ho:LuAG rod laser. *Laser Phys. Lett.* **2010**, *8*, 120–124. [[CrossRef](#)]
10. Chen, H.; Shen, D.; Zhang, J.; Yang, H.; Tang, D.; Zhao, T.; Yang, X. In-band pumped highly efficient Ho:YAG ceramic laser with 21 W output power at 2097 nm. *Opt. Lett.* **2011**, *36*, 1575–1577. [[CrossRef](#)] [[PubMed](#)]
11. Chao, C.; Ju, Y.L.; Yao, B.Q.; Dai, T.Y.; Duan, X.M.; Li, J.; Ding, Y.; Liu, W.; Pan, Y.B.; Li, C.Y. Passively Q-switched Ho:YLF laser pumped by Tm<sup>3+</sup>-doped fiber laser. *Opt. Laser Technol.* **2016**, *77*, 55–58.
12. Walsh, B.M.; Barnes, N.P.; Petros, M.; Yu, J.; Singh, U.N. Spectroscopy and modeling of solid state lanthanide lasers: Application to trivalent Tm<sup>3+</sup> and Ho<sup>3+</sup> in YLiF<sub>4</sub> and LuLiF<sub>4</sub>. *J. Appl. Phys.* **2004**, *95*, 3255–3271. [[CrossRef](#)]
13. Zhao, C.; Hang, Y.; Zhang, L.; Yin, J.; Hu, P.; Ma, E. Polarized spectroscopic properties of Ho<sup>3+</sup>-doped LuLiF<sub>4</sub> single crystal for 2  $\mu\text{m}$  and 2.9  $\mu\text{m}$  lasers. *Opt. Mater.* **2011**, *33*, 1610–1615. [[CrossRef](#)]
14. Walsh, B.M.; Grew, G.W.; Barnes, N.P. Energy levels and intensity parameters of Ho<sup>3+</sup> ions in GdLiF<sub>4</sub>, YLiF<sub>4</sub> and LuLiF<sub>4</sub>. *J. Phys. Condens. Matter* **2005**, *17*, 7643. [[CrossRef](#)]
15. Schellhorn, M. High-energy, in-band pumped Q-switched Ho<sup>3+</sup>:LuLiF<sub>4</sub> 2  $\mu\text{m}$  laser. *Opt. Lett.* **2010**, *35*, 2609–2611. [[CrossRef](#)]
16. Schellhorn, M. High-energy, in-band pumped Ho:LLF MOFA system. In *Advanced Solid-State Photonics*; Optical Society of America: Washington, DC, USA, 2012; p. AW4A-4.
17. Walsh, B.M. Dual wavelength lasers. *Laser Phys.* **2010**, *20*, 622–634. [[CrossRef](#)]
18. Vodopyanov, K.L.; Fejer, M.M.; Simanovskii, D.M.; Kozlov, V.G.; Lee, Y.S. Terahertz-wave generation in periodically-inverted GaAs. In *Proceedings of the Conference on Lasers and Electro-Optics*, Baltimore, MD, USA, 22–27 May 2005; p. CW11.
19. Xing-Peng, Y.; Qiang, L.; Hai-Long, C.; Xing, F.; Ma-Li, G.; Dong-Sheng, W. A novel orthogonally linearly polarized Nd:YVO<sub>4</sub> laser. *Chin. Phys. B* **2010**, *19*, 395–400. [[CrossRef](#)]
20. Jing Zhang, J.Z.; HuiLong Li, H.L.; Jing Xia, J.X.; Xihong Fu, X.F. Orthogonally polarized dual-wavelength Nd:YLiF<sub>4</sub> laser. *Chin. Opt. Lett.* **2015**, *13*, 37–42. [[CrossRef](#)]

21. Segura, M.; Kadankov, M.; Mateos, X.; Pujol, M.C.; Carvajal, J.J.; Aguiló, M.; Díaz, F.; Griebner, U.; Petrov, V. Polarization switching in the 2-m Tm:KLu(WO<sub>4</sub>)<sub>2</sub> laser. *Laser Phys. Lett.* **2012**, *9*, 104–109. [[CrossRef](#)]
22. Zhang, X.L.; Zhang, S.; Xie, Z.L.; Li, G.X.; Yu, L.; Cui, J.H.; Zhao, J.Q.; Li, L. Polarization switching and optical bistability in the diode-pumped Tm,Ho:LLF laser. *Laser Phys. Lett.* **2014**, *11*, 1528–1529. [[CrossRef](#)]
23. Zhang, X.; Zhang, S.; Wang, C.; Li, L.; Zhao, J.; Cui, J. Orthogonally polarized dual-wavelength single-longitudinal-mode Tm,Ho:LLF laser. *Opt. Express* **2013**, *21*, 22699–22704. [[CrossRef](#)]
24. Zhang, X.L.; Yu, L.; Zhang, S.; Li, L.; Zhao, J.Q.; Cui, J.H.; Dong, G.Z.; Wang, R. Controlled optical bistability switching in a diode-pumped Tm,Ho:LLF laser. *Laser Phys. Lett.* **2013**, *10*, 5801. [[CrossRef](#)]
25. Barnes, N.P.; Walsh, B.M.; Filer, E.D. Ho:Ho upconversion: Applications to Ho lasers. *J. Opt. Soc. Am. B* **2003**, *20*, 1212–1219. [[CrossRef](#)]
26. Kang, P.; Zhang, S.; Zhang, X.; Huang, J. High power self-Q-switched Tm:YAP solid state laser based on the ground state reabsorption. *Infrared Phys. Technol.* **2022**, *123*, 104117. [[CrossRef](#)]
27. Liu, H.; Cao, S.; Wang, W.; Lin, B.; Lu, W.; Fang, Z. A 1 $\mu$ m laser output based on an Er-doped fiber femtosecond laser. *Opt. Commun.* **2017**, *397*, 161–165. [[CrossRef](#)]
28. Wang, M.Q.; Ding, S.H.; Yu, W.Y.; Zhang, W.H. High-efficient diode-pumped passively Q-switched c-cut Nd:GdVO<sub>4</sub> self-Raman laser. *Laser Phys. Lett.* **2013**, *10*, 045403. [[CrossRef](#)]
29. Liu, J.; Yang, J.; He, J. High repetition frequency passively Q-switched diode-pumped Nd:YVO<sub>4</sub> laser. *Opt. Laser Technol.* **2003**, *35*, 431–434. [[CrossRef](#)]

**Disclaimer/Publisher's Note:** The statements, opinions and data contained in all publications are solely those of the individual author(s) and contributor(s) and not of MDPI and/or the editor(s). MDPI and/or the editor(s) disclaim responsibility for any injury to people or property resulting from any ideas, methods, instructions or products referred to in the content.